JMEPEG (1994) 3:619-634

Forming and Fractographical Characteristics of Copper-Nickel-Beryllium Sheets Under Tension and Bending

A.A. Tseng, T.C. Chen, K.P. Jen, and T. Ochiai

Formability and its fracture characteristics are critical factors in fabricating spring components from sheet base materials. Copper-nickel-beryllium (C17510) alloys provide excellent formability for producing highly reliable connectors used in electrical and electronic applications. The formability of a commercially available CuNiBe alloy was studied with emphasis on springback evaluations. Experiments were conducted to investigate the forming related tensile and bending properties. Fractographical examinations were conducted to identify the characteristics of failure and predict its initiation. Several analytical formulas for predicting springback are presented herein to provide a simple tool for computer-assisted design of spring components. To verify their reliability, the analytical predictions were first compared with the experimental data. Then predictions based on different formulations were compared with each other to identify an appropriate formula to be used in design of the highly reliable spring components.

Keywords

copper-nickel-beryllium alloys, forming, fractography, tensile properties

1. Introduction

COPPER-NICKEL-BERYLLIUM (CuNiBe) sheets have been used across a broad spectrum of applications, spanning the automotive, aerospace, electronics, appliance, and medical industries. The popularity of this alloy mainly results from its combination of high conductivity, good mechanical strength, and nonmagnetic characteristics (Ref 1, 2). The alloy is age hardenable to moderate strength levels with high electrical conductivity value and good formability. It normally contains ~0.5% Be in Cu. In this paper, a commercially available alloy, UNS No. C17510, also known as one of the ASTM B534 alloys, is considered (Ref 1). It is the material of choice in current carrying springs, thermal control devices, welding electrodes, and power connectors.

As the demand for high connection density in electrical and electronic products grows, springback behaviors become increasingly critical in the design and fabrication of these miniaturized contact components from sheet base materials (Ref 3, 4). This paper presents a study of the springback and other forming related properties of CuNiBe sheets with the goal of providing reliable information to help manufacturing or tool engineers in the production of these intricate electronic components. In general, sheet metals used in electronic parts are thin and subjected to relatively small strain; therefore, they are likely to experience considerable springback. This is particularly significant in bending and other bending related forming operations.

Both springback and bending formability (or bendability) are dependent on the material and geometric parameters involved, including composition, heat treatment, sheet thickness and width, and method of bending. Usually, springback and bendability can both be quantified by a V-shaped bending test, characterized by the final angle and the ability of the sheet to be bent without cracking, respectively. Springback is a measure of the amount of elastic recovery upon removal of the load during bending and must be compensated for in tooling. Normally, a part that was bent at an angle will have a final one greater than the angle bent. The present study is expected to lead to the discovery of specific parameters that could reliably correlate the sheet springback behavior in forming electronic components. With this information, appropriate tooling can be designed to compensate for the springback, such as overbending the sheet. Other antispringback measures, including bottoming, stretch bending, and double bending, could also be used (Ref 5, 6).

Bendability is determined by the ability of the sheet to be bent to a required geometry without cracking or failure. The V-shaped bending tester presently used consists of a 90° V-shaped block and 90° punches with various radii ground into the leading edge as shown in Fig. 1. Following bending, the sample surface is examined for cracks on the convex side of the radius. If no cracks are visible, the sample passes the test at that radius. The punch radius is then reduced, and another sheet sample is tested. This procedure is repeated until cracks appear in the sample surface. The smallest radius, R, not to cause visible cracking is divided by the sheet thickness, t, to determine the R/t ratio. Sheet bendability is rated by this R/t ratio (Ref 5, 6).

The present research studies three aspects of the CuNiBe sheets. First, a study of the tensile properties of CuNiBe sheets, including the yield and ultimate strengths, percent elongation, and elastic modulus, is presented. The parameter of the strain-hardening exponent, which has often been used to quantify the stretch formability, is also evaluated. Second, the springback behavior is studied. Analytical formulas are developed to predict the springback behavior; bending testing also is performed

A.A. Tseng, Department of Mechanical Engineering and Mechanics, Drexel University, Philadelphia, PA 19104, USA; **T.C. Chen,** Department of Mechanical Engineering and Mechanics, Drexel University, Philadelphia, PA 19104, USA, on sabbatical leave from National Cheng Kung University, Tainan, Taiwan; **K.P. Jen,** Mechanical Engineering Department, Villanova University, Villanova, PA 19085, USA; **T. Ochiai,** NGK Metals Corp., Reading, PA 19612, USA

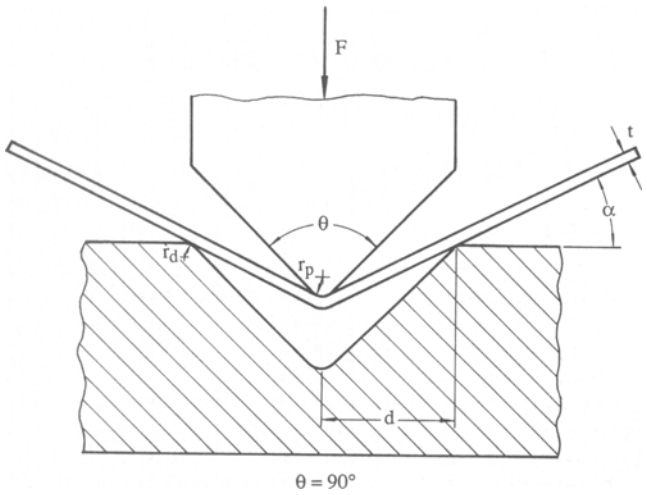

Fig. 1 Schematic diagram of v-shaped bend test

Table 1 Typical physical properties of alloy C17510

Liquidus temperature	1070 °C (1958 °F)(a)
Solidus temperature	1004 °C (1840 °F)
Density at 20 °C	8.78×10^{-3} kg/cm^3 (0.317 lb/in.^{3})
Thermal expansion coefficient at 20 to 200 °C	17.8×10^{-6} K^{-1} (10.0×10^{-6} °F^{-1})
Thermal conductivity at 20 °C	208 W/m · K (120 Btu/ft · h · °F)
Electrical conductivity at 20 °C (IACS)	45 to 48%
Specific heat at 20 °C	419 J/kg · K (0.1 Btu/lb · °F)
Modulus of elasticity	132 GPa (19.2×10^6 psi)
Modulus of rigidity	52 GPa (7.5×10^6 psi)
Poisson ratio	0.345

(a) US customtary units

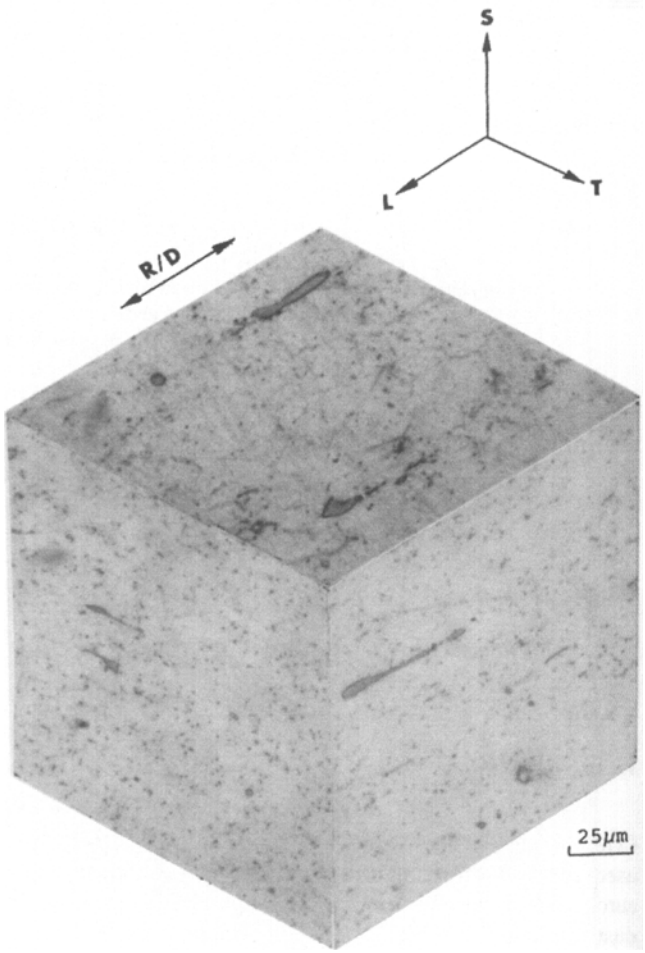

Fig. 2 3-D optical micrographs showing beryllide particles and stringers (unetched)

to provide springback measurements. The experimental measurements are used not only to verify the analytical prediction, but also to quantify the bendability of the CuNiBe sheets tested. Finally, springback information needed for the design of connection components is discussed. Optical metallurgical microscopes and scanning electron microscopes (SEM) are used to study the microstructure of the fractured tensile and bending specimens in order to identify the failure mechanism and crack initiation.

2. Microstructure

A batch of the C17510 sheets containing a nominal 0.4% Be and 1.8% Ni was selected for evaluation. The sheets were fully annealed, cold rolled, and precipitation treated, also known as HT or TH04 temper (Ref 1). The C17510 alloy is a high electrical and thermal conductivity copper alloy exhibiting exceptional resistance to stress relaxation at elevated temperatures. Increasing aging temperature reduces the time to reach peak strength and decreases the achievable strength. As time increases, elongation falls while strength increases markedly. Beyond two hours, the rate of change in ductility becomes negligible. The physical properties of the alloy are summarized in Table 1.

Both optical and scanning electron microscopes were used to characterize the microstructure of the C17510 CuNiBe sheet. Figures 2 and 3 show two three-dimensional microstructures of the alloy sheet. Figure 2 is the microstructure right after polishing (prior to etching). It reveals small particles randomly distributed in the matrix and many elongated stringers parallel to the rolling direction. These small particles are believed to be beryllide phase, which is formed by the strong affinity between beryllium and nickel/cobalt element (Ref 7). Figure 3 shows the microstructure of the alloy after etching. It shows that strain hardening is induced because the grains are elongated in the rolling direction. Many twins are observed in the elongated grains. The striations on the top surface of Fig. 3 are caused by metastable precipitates, which are not resolved by the optical microscopy (Ref 7). The etchant used in Fig. 3 consists of 15 mL NH_4OH, 15 mL H_2O_2, 15 mL H_2O, and 4 pellets of NaOH (Ref 8). The etching time was ~12 s to obtain a proper contrast for the grain boundaries.

Small particles and stringers can be shown more clearly using the SEM as shown in Fig. 4 (back scattering electron image). In general, the stringer forms a fine line, with a thickness

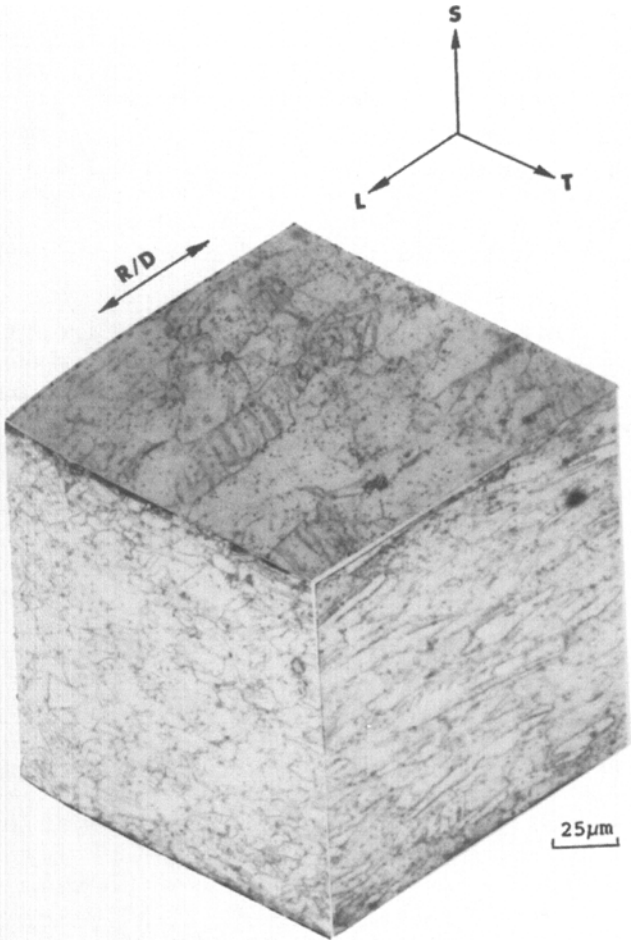

Fig. 3 3-D optical micrographs showing grain structures (etched)

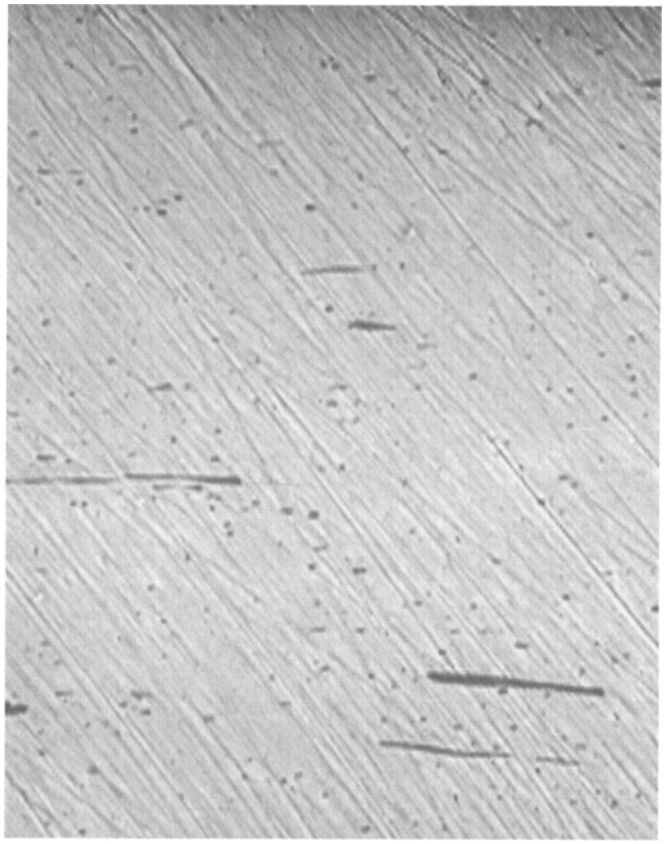

Fig. 4 Back scattering image showing particles and stringers

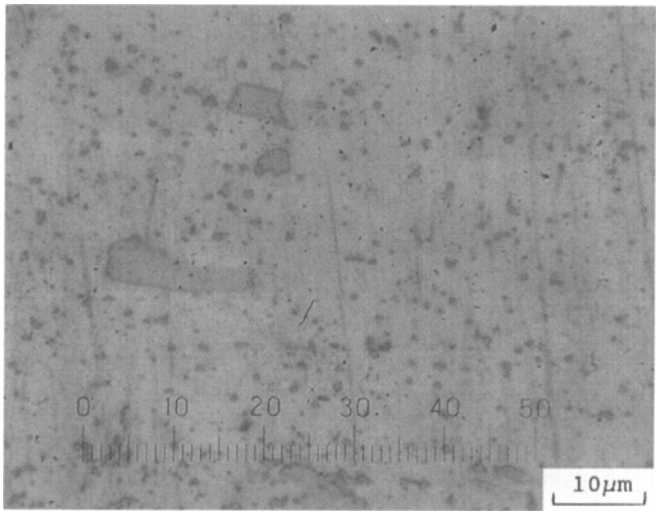

Fig. 5 Optical micrograph showing beryllide particles and stringers

of ~1 micron. However, many larger stringers with a tadpole shape exist in the alloy. Figures 2 to 4 show that stringers can be as large as $10 \times 5 \times 2$ microns, and they are elongated along the rolling direction. Microanalysis from EDS (energy dispersive spectrometer) shows that stringers are rich in Co and Ni. Due to the significant size difference between the particles and stringers, initially, they were thought to be two different phases in the microstructure. However, using cyanide as the etchant (Ref 7), both the stringers and particles showed the same blue-gray color at higher magnification as shown in Fig. 5. It was concluded that both particles and stringers are beryllide. The stringers later were identified to be detrimental to the specimens under tensile load because cracks tend to develop at the stringers.

3. Tensile Testing

The uniaxial tensile test is the most frequently used test to determine the mechanical properties of metals. The test provides information that can be used in component design, quality control of the product, and process control of operations. The test itself is relatively simple, but interpretation and use of the test data for CuNiBe alloys require specific attention to the alloy's behavior during testing.

3.1 *Procedure*

In testing, the procedures recommended by the ASTM Standard E 8 (Ref 9) were followed. Several properties from

Table 2 Tensile properties of C17510 sheets

Alloy	UNS No.	Young's modulus, E		Yield strength, Y		Predicted yield strength		Ultimate strength		Elongation,	Predicted yield strain, %
		GPa	10^6 psi	MPa	ksi	MPa	ksi	MPa	ksi	%	
3-TH04-T(a)	C17510	116.41 ± 2.85	16.88 ± 0.41	795.22 ± 5.94	115.3 ± 1.89	798.76	115.85	840.01 ± 4.74	121.8 ± 0.69	12.07 ± 0.17	0.686
3-TH04-L(b)	C17510	117.66 ± 2.85	17.06 ± 0.41	821.88 ± 5.16	119.2 ± 0.75	830.81	120.49	889.42 ± 6.17	129.0 ± 0.89	8.60 ± 0.34	0.706

(a) Transverse direction. (b) Longitudinal direction

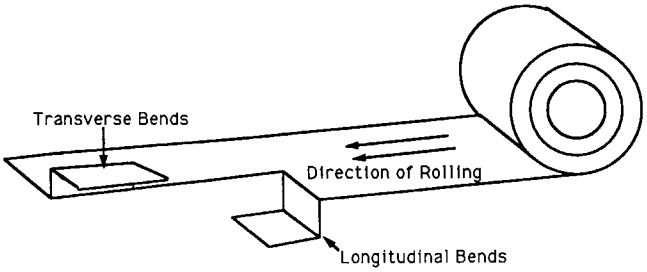

Fig. 6 Rolling and bend test convention

the stress-strain curve were used in an attempt to evaluate the forming related properties, including strain hardening, elastic modulus, anisotropy, and ductility (or percent elongation). All of these properties were evaluated.

Testing specimens were cut from two directions: longitudinal and transverse. Ten specimens were prepared for each batch; five specimens were tested for each direction. The convention for the rolling (longitudinal) direction and bend orientation is shown in Fig. 6. The specimens were stamped by a dog-bone-shaped die in a TINIUS OLSEN press, Tinius Olsen Testing Machine Co., Inc., Willow Grove, PA, with the dimensions specified in the ASTM Standard. After stamping, the edges of the stamped specimens were also ground by grid No. 600 sandpaper to remove burr. Before testing, the dimensions of the specimens were measured by a micrometer, and a 51-mm (2-in.) gage length was then marked on each specimen.

A universal tester, model 1125, was used for tensile testing. Before the test, the Instron 6059 extensometer, Instron Corporation, Canton, MA, with 51-mm gage length and 25-mm max extension was calibrated according to the ASTM Standard. The testing specimen was attached to the load cell by wedge grips. The extensometer was attached at the 50-mm gage mark of the specimen. The cross head speed was set to 1.27 mm/min (0.05 in./min), and the load cell was set to 2.2 kN (500 lb) maximum load. The strain range was set to 12.5-mm max extension, and the specimen was loaded until final fracture. The testing results of the load versus elongation were plotted in an Instron recorder.

The tensile strength and 0.2% yield strength were calculated directly from the load versus elongation curve. The former was based on the maximum load; the latter was from a 0.2% offset of the linear elastic part of the curve. The percent elongation was obtained from the elongation at fracture. The percent elongation was double checked by measuring the real extension of the fractured specimen. Young's modulus was the slope of the linear elastic part of the curve in which the increment of stress was divided by the corresponding increment of strain. In order to increase the accuracy of Young's modulus, the strain gage was adjusted to a higher sensitivity representing 0.25% strain for every 25.4-mm chart movement.

3.2 *Tensile Properties*

The C17510 sheets were evaluated in both the longitudinal (rolling) and transverse directions. The results for the tensile properties are summarized in Table 2, including Young's modulus, yield strength, ultimate strength, and percent elongation. All data were based on at least five testings. In the table, the values before the plus/minus sign are the arithmetic means, and following the sign are the corresponding standard deviations. As shown, the standard deviations of the ultimate and yield strengths are within 1% of the mean value; this indicates that the experimental data are exceptionally consistent. For the percent elongation and elastic modulus, their standard deviations depart from the mean value within 4%, which means that the testing data are reasonably consistent and reliable.

Table 2 shows that the tensile and yield strengths in the longitudinal direction are ~5% higher than those in the transverse direction. The percent elongation or ductility in the transverse direction is ~25% higher than that in the longitudinal direction. However, the moduli of elasticity in both directions were very close to each other, although the longitudinal direction was slightly higher. Typically, the longitudinal tensile strength is higher than that in the transverse direction because the strain hardening was induced in this direction during the rolling process. Conversely, ductility is higher in the transverse direction if the surface finish is appropriate. Any deep rolling marks on the sheet surface may cause stress concentrations, which are more significant for a transverse specimen.

3.3 *Strain Hardening and Formability*

The engineering stress-strain curves were also converted to the true stress-strain relationships. More than 30 points were selected from a load versus elongation curve. The corresponding load versus elongation data were then reconstructed to the true stress-strain curves following the formula recommended by the ASTM E 646 Standard (Ref 10). If the stress/strain behavior follows a power-law relationship, the strain-hardening exponent, n, and the strength coefficient, K, are the slope and intercept of the stress-strain curve, which is close to a straight line plotted in a log-log scale. Each n and K value is calculated, respectively, based on slopes and intercepts of the straight curve fit to a range of data. Hence, standard deviations were

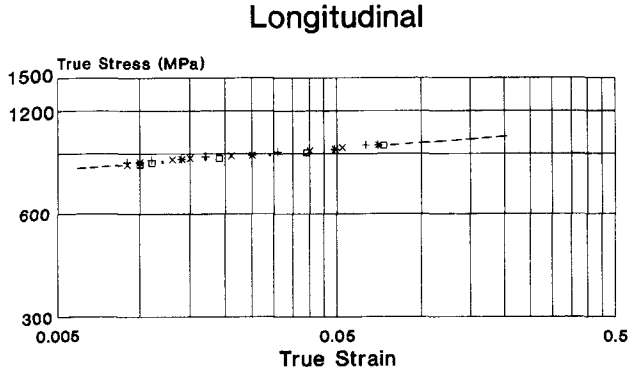

Fig. 7 Stress-strain curve in logarithmic-scale coordinates for longitudinal direction

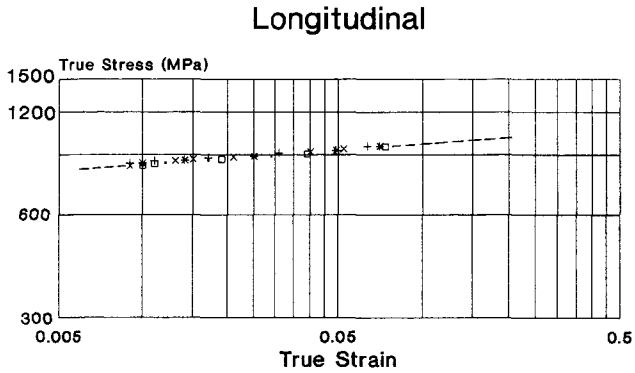

Fig. 8 Stress-strain curve in logarithmic-scale coordinates for transverse direction

Table 3 Strain hardening properties of C17510 sheets

Alloy	Strain range	Strain hardening exponent, n	Strength coefficient, K MPa	Strength coefficient, K ksi
C17510-TH04-T(a)	0.010 to 0.100	0.050 ± 0.005	1024.7 ± 20	148.6 ± 2.9
C17510-TH04-L(b)	0.009 to 0.070	0.059 ± 0.002	1112.8 ± 5	161.4 ± 0.8

(a) Transverse direction. (b) Longitudinal direction

calculated based on this variance of data about the fitted line. Mathematical representation for a power-law curve is:

$$\sigma_e = K\varepsilon_e^n \quad \text{(Eq 1)}$$

where σ_e is the uniaxial or effective stress and ε_e is the uniaxial or effective strain.

The stress-strain curves for C17510 sheets are shown in Fig. 7 and 8 for the longitudinal and transverse directions, respectively. As shown, the data follows the power-law relationship very well. The corresponding arithmetic means and standard deviations of the strain-hardening exponent, n, and strength coefficient, K, are reported in Table 3. As shown, in the transverse direction, the standard deviations for n and K are <10% and <2% of the means, respectively. The results for the longitudinal direction are much better; the corresponding deviations are 3.5% and 0.5%, respectively. This indicates that the true stress-strain behavior of the CuNiBe sheets closely follows a power-law behavior and can be reasonably quantified by a single value of the strain-hardening exponent, n. Note that, in many materials, the instantaneous value of n can be a function of the strain, and within a reasonable accuracy, i.e., the standard deviation within 10% of the mean value, two distinct n values are needed to describe the strain hardening behavior (Ref 4, 10).

The exponent, n, is one measure of strain-hardening ability. In materials with high n values, localized deformation causes a rapid increase in strength with the result that the highly strained areas resist further deformation, and subsequent deformation is transferred to adjacent, less strained, areas. As a result, strains are uniformly distributed over a large area. In materials with low n values, strains are concentrated rather than being distributed over the area being deformed. Subsequently, the concentrated strain causes thinning until ultimate failure occurs. Roughly speaking, the parameter n represents the resistivity of strain concentration and mainly depends on material composition. The material with the higher n value gives a more uniform strain distribution; hence, there is less chance that it will tear during stretching (Ref 4, 11).

3.4 *Fractography*

The SEM was used to investigate the fracture surface of the tensile specimens. The fracture surfaces of all specimens reveal ductile fracture behavior. In general, the fracture surface is along a plane ~45° to the loading direction. Shear dimple is the major feature on the fracture surfaces regardless of the types of specimen (Fig. 9). Shear dimples, shearing toward the rolling surface, are nucleated from the beryllide particles where the microvoids are formed. Occasionally, a few conical equiaxed dimples are observed on the transverse tensile specimens. Figure 9(b) shows that fracture surfaces contain many cracks that are parallel to the rolling surface. These cracks are longer on the fracture surface of the transverse specimen than that of the longitudinal specimen. In fact, these cracks develop at the beryllide stringer sites, which are parallel to the rolling direction.

The Ni/Co beryllide stringers were not readily visible because they tend to dislodge from the fracture surfaces. Figure 10 shows that no dimples exist and very little plastic deformation is available near a stringer site. It clearly indicates that stringers would decrease the tensile strength because cracks tend to develop at stringer sites due to the inhomogeneity in the materials. This effect is more significant in the transverse tensile specimen because the stringers are normal to the loading direction.

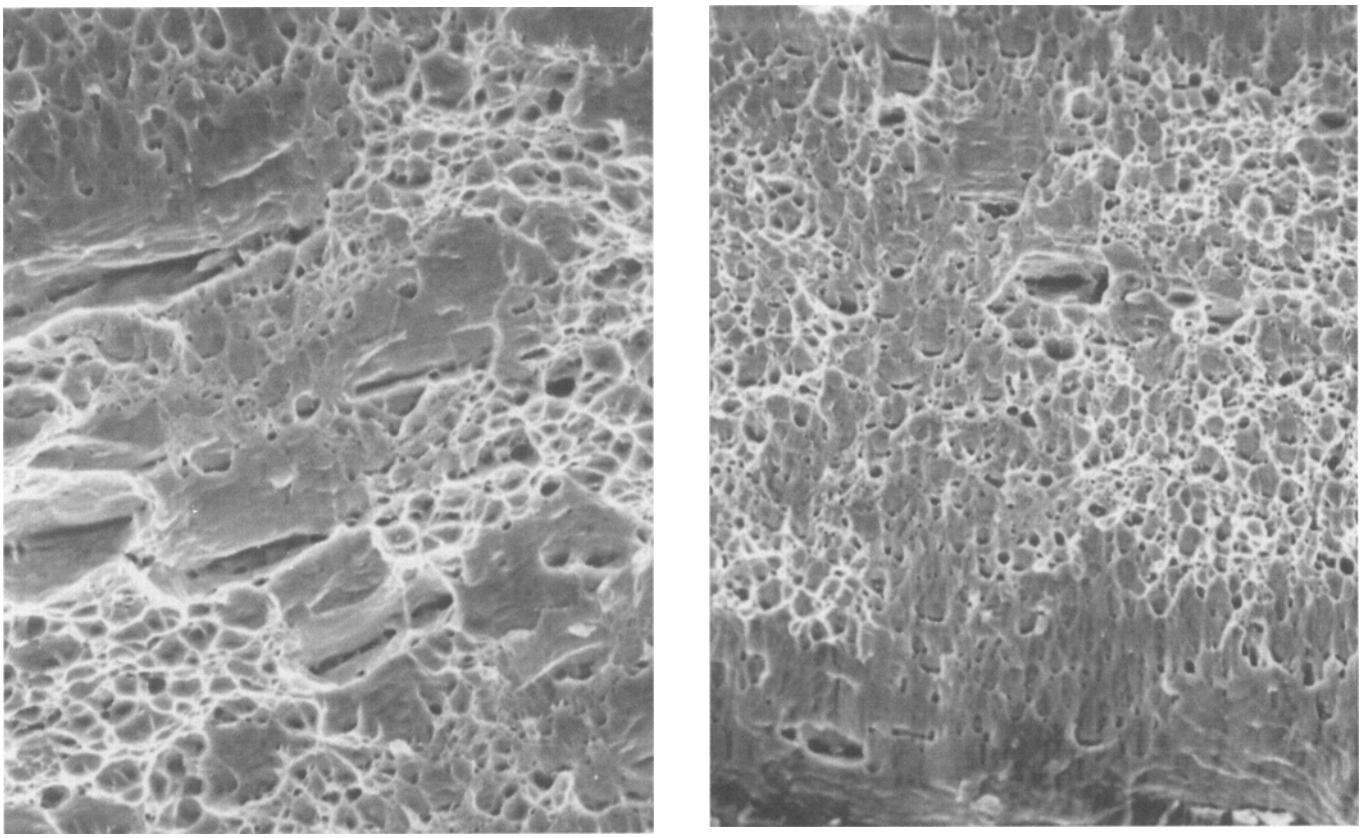

(a) (b)

Fig. 9 SEM fractograph showing shear dimples of tensile specimens. (a) Longitudinal. (b) Transverse

3.5 *Modified Yield Strength*

If a power-law is used to represent the true stress-strain behavior, the intersection of the power-law curve and Young's modulus line can be considered as the yield strength, theoretically. In this paper, this strength is called the predicted or calculated yield strength, σ_y, and can be found as (Ref 12):

$$\sigma_y = K(K/E)^{n/(1-n)} \quad \text{(Eq 2a)}$$

where E is the Young's modulus. The corresponding yield strain, ε_y, can also be calculated based on the predicted σ_y value:

$$\varepsilon_y = \sigma_y/E = (K/E)^{1/(1-n)} \quad \text{(Eq 2b)}$$

The calculated σ_y and ε_y values are listed in Table 2; there is no significant difference between the measured value, Y, and σ_y in both directions.

4. Springback Formulation

All sheet-forming operations incorporate some bending. As indicated in the results from the tensile tests, the stress-strain behavior of the CuNiBe sheets closely follows a power-law behavior, quantified by the strain-hardening exponent, n, and strength coefficient, K. The springback formula developed for the CuNiBe sheets should have the capability to predict springback for this type of constitutive relationship. In the present study, an analytical solution based on a power-law relationship is, therefore, developed to estimate the springback during bending.

4.1 *Stresses and Strains*

The analytical solution is developed based on the condition that a flat sheet with power-law strain-hardening is subjected to a bending deformation. It is assumed that the width of the workpiece is large compared to the thickness, t, so that the conditions of plane strain apply. As the punch descends, the contact forces at the die corner produce a bending moment at the punch corner of sufficient magnitude to permit the necessary deformation, as shown in Fig. 1. The bending stresses are compressive above the neutral axis and tensile below; their magnitudes are shown in Fig. 11. For a von Mises material under a plane-strain condition, the bending stress, σ_b, is:

$$\sigma_b = (4/3)^{1/2}\,\sigma_e \quad \text{(Eq 3)}$$

In plane-strain bending, the relationship between the effective strain, ε_e, and the bending strain, ε_b, for a von Mises material is:

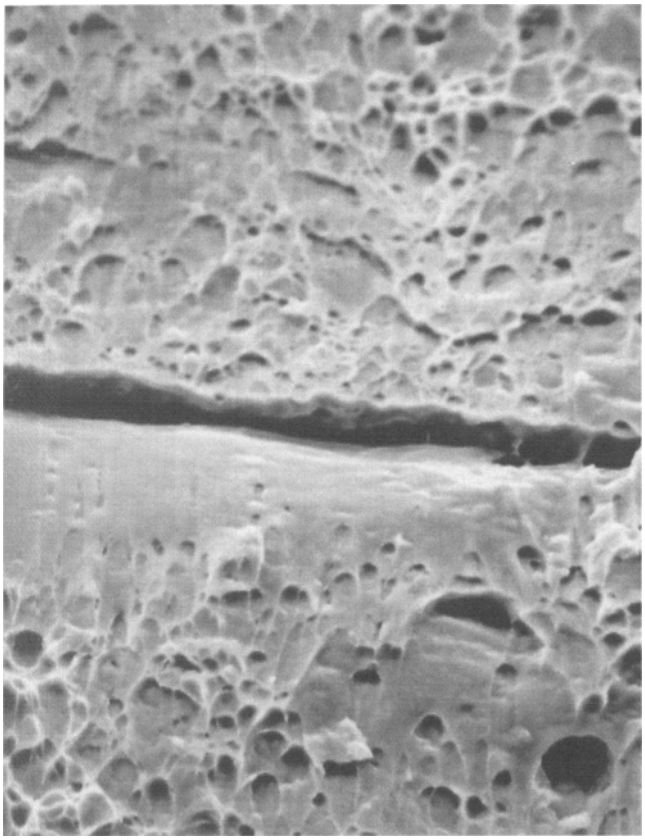

Fig. 10 SEM fractograph showing little plastic deformation near the stringer sites

$$\varepsilon_e = (4/3)^{1/2}\,\varepsilon_b \qquad \text{(Eq 4)}$$

Substituting Eq 1 into Eq 3 and replacing ε_e by ε_b by using the relationship given in Eq 4, Eq 3 becomes:

$$\sigma_b = (4/3)^{1/3}\,\sigma_e = (4/3)^{(n+1)/2} K\,\varepsilon_b{}^n \qquad \text{(Eq 5)}$$

Let r be the radius of curvature measured to the neutral plane and z be the distance of any element from the neutral plane in the thickness direction; the bending strain, ε_b, at z can be found to be z/r. Substituting ε_b by z/r, the above equation becomes:

$$\sigma_b = (4/3)^{(n+1)/2} K(z/r)^n \qquad \text{(Eq 6)}$$

The above stress distribution across the sheet thickness is used to calculate the bending moment. Note that although the strain in bending is not necessarily small, in order to simplify the formulation, the expression of the engineering strain is adopted here.

4.2. *Bending Moments*

From the classic beam theory, the resulting bending moment per unit width is:

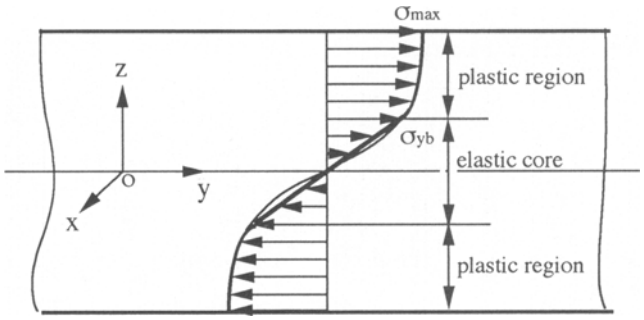

Fig. 11 Stress distribution of power-law materials under bending

$$M_b = 2\int_0^{t/2} \sigma_b\, z\, dz \qquad \text{(Eq 7)}$$

Substituting Eq 5 into the above equation, the unit bending moment becomes:

$$M_b = 2\int_0^{t/2} (4/3)^{(n+1)/2} K(z/r)^n\, z\, dz$$
$$= 2(4/3)^{(n+1)/2} K(t/2)^{n+2} / [(n+2)r^n] \qquad \text{(Eq 8)}$$

4.3 *Springback*

For a bending process, the springback is estimated after the curved portion has been formed under the action of M_b. The unloading process is an oppositely directed M_b or M_{unload}, applied so that the total load is zero, and the material is elastically deformed under unloading. The difference of deformation between being loaded by M_b and unloaded by the oppositely directed M_{unload} is the springback. Figure 12 shows the portion that has been plastically deformed at a strain of z/r, and the strain, $\Delta\varepsilon_y$, that is subject to the oppositely directed moments is:

$$\Delta\varepsilon_b = z/r - z/r' \qquad \text{(Eq 9)}$$

where r' is the final strain or strain after springback. Under elastic plane strain deformation, the stress/strain relationship is:

$$\Delta\sigma_b = [E/(1-\upsilon^2)]\,\Delta\varepsilon_b \qquad \text{(Eq 10)}$$

where E is the Young's modulus and υ is the Poisson ratio. Because the sheet is elastically deformed under unloading, the above relationship can be used to calculate the bending stress. Consequently, with the formula given in Eq 7, the oppositely directed M_{unload} is:

$$M_{\text{unload}} = 2E/(1-\upsilon^2)\int_0^{t/2} \Delta\varepsilon_b\, z\, dz$$
$$= E\,t^3(1/r - 1/r')/[12\,(1-\upsilon^2)] \qquad \text{(Eq 11)}$$

As mentioned, after unloading, the resultant load should be zero; i.e., $M_b - M_{\text{unload}} = 0$. Thus:

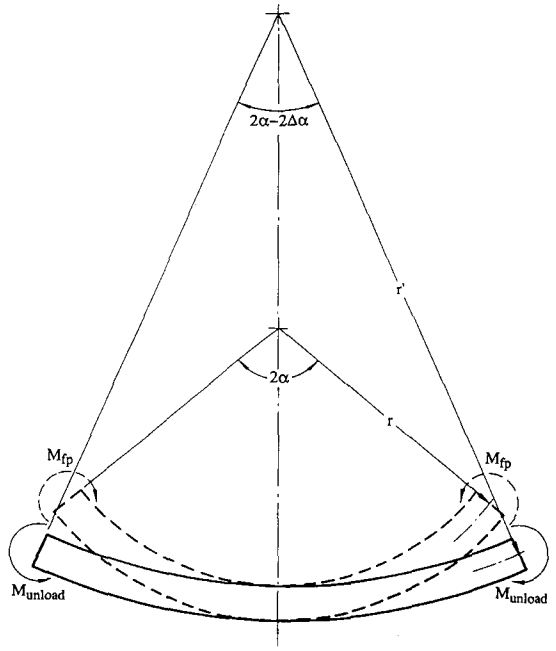

Fig. 12 Schematic description of springback resulted from opposite moments M_{unload}

$$M_b = M_{\text{unload}} = E\,t^3\,(1/r - 1/r')\,/\,[12\,(1-\upsilon^2)] \qquad \text{(Eq 12)}$$

As shown in Fig. 11, the bend angle, 2α, reduces to $2\alpha - 2\Delta\alpha$ after the springback. Now the springback factor, also known as the springback ratio, K_S, can be expressed as:

$$K_S = (\alpha - \Delta\alpha)\,/\,\alpha = r\,/\,r' \qquad \text{(Eq 13)}$$

4.4 *Springback Factor for a Sheet Neglecting Elastic Core Effect*

While $K_S = 1$ indicates no springback, $K_S = 0$ implies complete springback. Substituting Eq 12 into the above equation and letting $r = r_p + t/2$, the springback factor, K_S, becomes:

$$K_S = 1 - 12\,(1-\upsilon^2)\,(r_p + t/2)\,M_b\,/\,(E\,t^3) \qquad \text{(Eq 14)}$$

where r_p is the punch radius, as shown in Fig. 1. Substituting Eq 8 into the above equation gives:

$$K_S = 1 - 3(4/3)^{(1+n)/2}\,(K/E)\,(1-\upsilon^2)\,[(2r_p/t) + 1]^{1-n}/(2+n) \qquad \text{(Eq 15)}$$

The above derivation is essentially similar to that presented by Hosford and Caddell (Ref 12), in which their formula predicted the final curvature of a bent sheet. In the present study, however, the springback factor and springback angle are directly formulated.

4.5 *Springback Factor for Beam Bending (Plane Stress Condition)*

A similar development can also be made for the plane stress condition, a circumstance close to bending a relatively narrow beam. The corresponding springback factor for plane stress bending can be found through replacing $E/(1-\upsilon^2)$ with E and $K(4/3)^{(1+n)/2}$ with K in Eq 15:

$$K_S = 1 - 3\,(K/E)\,[(2r_p/t) + 1]^{1-n}\,/\,(2+n) \qquad \text{(Eq 16)}$$

The difference of springback between bending a narrow beam, Eq 16, and a wide sheet, Eq 15, is discussed in section 6, Bending Results.

4.6 *Springback Factor for Sheets with an Elastic Core*

As shown in Fig. 11, near the core region, the sheet is deformed elastically, and a linear equation instead of the power-law curve of Eq 1 should be used for the stress-strain relationship. The bending stress distribution in the elastic region is:

$$\sigma_b = [E/(1-\upsilon^2)]\,\varepsilon_b \qquad \text{(Eq 17)}$$

Here $0 \le \varepsilon_b \le \varepsilon_{yb}$, and ε_{yb} is the yield strain under plane strain bending, which is located on the boundary between the elastic core and plastic regions (Fig. 11). Using the relationship developed in Eq 2b, the plane-strain yield strain, ε_{yb}, is (Ref 13):

$$\varepsilon_{yb} = (1-\upsilon^2)\,\varepsilon_y\,/\,(1-\upsilon+\upsilon^2)^{1/2} = (1-\upsilon^2)\,(K/E)^{1/(1-n)}\,/\,(1-\upsilon+\upsilon^2)^{1/2} \qquad \text{(Eq 18)}$$

Substituting Eq 17 into Eq 7, the bending moment by stresses in the elastic region, M_e, is:

$$M_e = 2E\,r^2\,\varepsilon_{yb}^3\,/\,[3\,(1-\upsilon^2)] \qquad \text{(Eq 19)}$$

Following the procedures developed earlier for the power-law sheets, the moment in the plastic region, M_p, is:

$$M_p = 2K(4/3)^{(1+n)/2}[(\varepsilon_{\max})^{n+2} - (\varepsilon_{yb})^{n+2}]\,/\,(n+2) \qquad \text{(Eq 20)}$$

where $\varepsilon_{\max} = t/(2r)$ and $\varepsilon_{yb} \le \varepsilon_b \le \varepsilon_{\max}$. The total bending moment, M_b becomes $M_e + M_p$, and K_S is:

$$K_S = 1 - 3\,(K/E)\,(1-\upsilon^2)\,[(2r_p/t) + 1]^{1-n}/[(2+n)(3/4)^{(1+n)/2}] + [(2r_p/t) + 1]^3(K/E)^{3/(1-n)}[3(4/3)^{(1+n)/2}(1-\upsilon^2)^{2+n}]/[(2+n)(1-\upsilon+\upsilon^2)^{(2+n)/2}] - (1-\upsilon^2)^2/[(1-\upsilon+\upsilon^2)^{3/2}] \qquad \text{(Eq 21)}$$

The above formulation is much more complicated than that of Eq 15. The result difference between these two equations is assessed.

4.7 *Springback Factor Based on True Strain Expression*

A linear relationship between strain and deformation or the engineering strain is assumed for all of the above formulations; i.e., $\varepsilon_b = z/r$, as indicated in Eq 6. However, for a sheet under large deformation, the relationship between strain and displacement becomes nonlinear, and the expression of the true strain should be adopted:

$$\varepsilon_b = \ln(1 + z/r) = z/r + (z/r)^2/2! + (z/r)^3/3! + \text{- - - - -} \quad \text{(Eq 22a)}$$

and

$$dz = r \exp(\varepsilon_b)\, d\varepsilon_b \quad \text{(Eq 22b)}$$

The maximum strain, ε_{max}, occurs at the outer layer of the sheet:

$$\varepsilon_{max} = \ln(1 + t/2r) = \ln[1 + t/(2r_p + t)] \quad \text{(Eq 23)}$$

If the nonlinear strain expression is used, the bending moment in the plastic region is:

$$M_p = 2K(2/\sqrt{3})^{n+1} r^2 \exp(2\varepsilon_{yb}) \times \sum_{j=0}^{\infty} [2^j - \exp(-\varepsilon_{yb})](\varepsilon_{max} - \varepsilon_{yb})^{n+j+1} / [j!\,(n+j+1)] \quad \text{(Eq 24)}$$

where ε_{yb} and ε_{max} are given in Eq 18 and 23, respectively. Again, following the procedures developed for Eq 14, the springback factor, K_S, is:

$$K_S = 1 - 12(1 - \upsilon^2)(r_p + t/2)(M_e + M_p)/(E\,t^3) \quad \text{(Eq 25)}$$

where M_e and M_p are given in Eq 19 and 24, respectively. Here, because the bending strain in the elastic core region is still relatively small, the engineering strain or the linear expression of strain is still applied. The expression of the springback factor can become somewhat lengthy if the explicit forms of M_e and M_p are substituted into Eq 25. The series in the above equation converges very rapidly. Only two to three terms are enough to provide convergent results; the convergence rate is assessed later. Again, the difference between the above formulation and Eq 15 is also discussed.

4.8 *Springback Angle*

Sometimes, the springback is characterized with respect to the punch angle, θ (Ref 2, 5, 6, 12). Because the punch or die angle, θ, equals $\pi - 2\alpha$ and $\Delta\theta = 2\Delta\alpha$, as shown in Fig. 1 or 12, the springback angle, $\Delta\theta$, with respect to the punch angle, can be directly obtained from the springback factor, K_S, through:

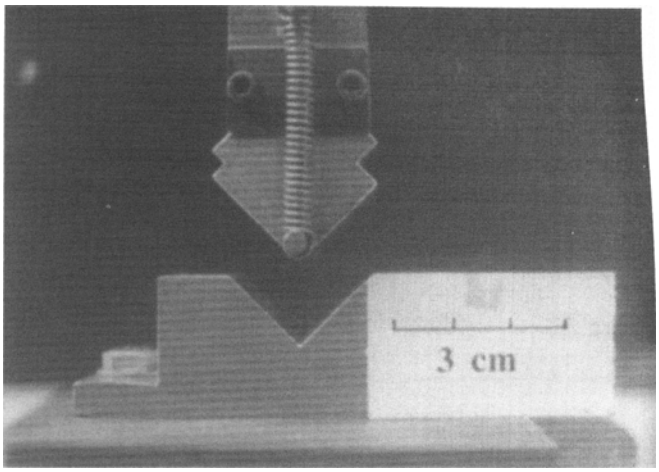

Fig. 13 Laboratory v-shaped bend tester

$$\Delta\theta/\theta = (\pi/\theta - 1)(1 - K_S) \quad \text{(Eq 26)}$$

Note that the above type of analysis assumes that the sheet part was initially bent through an angle of 2α (or $\pi - \theta$) as shown in Fig. 12. For $\theta = 90°$, the above equation becomes $\Delta\theta/90° = (1 - K_S)$ or $K_S = 1 - \Delta\theta/90°$.

5. Bending Testing

In this section, a piece of bending apparatus used for evaluation of the springback is introduced. The testing procedures are also presented.

5.1 *Apparatus Design*

A bend tester having a 90° V-shaped die and punch is selected to study the springback characteristics of the CuNiBe sheets. Since the springback behavior is highly dependent on the parameter of the r_p/t ratio, a wide range of r_p/t ratios must be examined. As a result, punches with various edge radii (r_p) have to be fabricated. To save the cost of punch fabrication and time needed for punch change, a test fixture having one punch to accommodate four to eight edge radii has been designed. As shown in Fig. 13, the test fixture consists of four main parts: press, interchangeable punch block, die, and cylindrical pins.

The punch is a 25.4-mm (1-in.) cube block made of steel having four square grooves. They were machined from the corners of the punch block with the dimensions being equal to the diameter of the cylindrical pin to be placed in it, as shown in Fig. 13. The cylindrical pins, made by Meyer Gage, Meyer Gage Co., Inc., South Windsor, CT, are actually used for gaging having 10 μm or better finish. They are available in diameters varying from 0.2794 mm (0.011 in.) to 12.7 mm (0.5 in.), thus permitting the experiment to be carried out for a wide range of r_p/t. The cylindrical gaging pins are made of steel and heat treated to a hardness of 60/62 Rockwell "C" with a 0.005 mm tolerance.

The gages are held in place in the groove by springs that also connect the gage to the movable pillar of the press. For the smaller gages, springs with a lesser spring stiffness are used in

order to ensure that the gage is not bent by too severely by a spring. Because the sheet considered is relatively thin, to have an accurate r_p/t ratio, the punch radius has to be controlled to a very tight tolerance. The use of the cylindrical gages provides not only the accommodation for different punch radii, but also the needed accuracy.

The press is an arbor press consisting of a main body, movable pillar, and base. The punch is mounted onto the pillar. A 90° V-shaped die having a 25.4-mm die span (2d in Fig. 1) is mounted onto the base of the press by two bolts. A hand lever arm is connected to the pillar by a gear arrangement and moves the punch to touch the die, thus bending the sheet to 90°.

5.2 *Testing Procedure*

In testing, the specimen sheet is cut ~25-mm wide and 75-mm long and placed on the surface of the die. The lever arm is used to move the pillar with the punch until the punch bottoms and comes in contact with the die, where it is held firm for at least 5 s and then released. With the setup described above, the cylindrical gages can be changed, thus varying the radius of the punch. If the bend radius is too sharp, excessive tensile strain on the outside surface may cause failure. Sometimes buckling, due to excessive compressive strain, is encountered on the inside of a bend.

Before testing, the dimensions of each specimen are measured and the punch radius is recorded. The thickness is measured with a micrometer (accurate to four decimal places) in three places, and an average is used. After the specimen is bent, the final angle (after springback) is measured from a pencil-traced outline of the bent sheet. Then the springback factor, K_S, is calculated. The experiment is performed in a similar manner for the varying punch radii, and a curve is plotted for K_S versus r_p/t.

6. Bending Results

6.1 *Springback Results*

The springback characteristics of the CuNiBe sheets were experimentally studied in both the longitudinal and transverse bend directions. The sheet specimen is ~0.15 mm thick. The bend test was performed for varying radii of punch, keeping the r_p/t ratio in a range from 2 to 15. At least three specimens are tested at each r_p/t ratio; all data reported are the arithmetic mean.

The springback measurements are shown in Fig. 14 and 15. In Fig. 14, the measurements are compared with the analytical predictions from Eq 15, while in Fig. 15, predictions based on Eq 25 are compared. The springback factor, K_S, versus the ratio of the punch radius to sheet thickness, r_p/t, is plotted. The sheets were evaluated in the longitudinal and transverse directions. Whereas K_S equal to 1 indicates no springback, K_S equal to zero implies complete springback or complete elastic recovery. In other words, the lower the springback factor, K_S, the higher the springback ($\Delta\theta$ in Eq 26). The data indicate that the higher the r_p/t ratio, the lower the K_S value. The predictions are calculated based on the materials properties provided in Tables 1, 2, and 3, including the Poisson ratio, strain-hardening exponent, strength coefficient, and Young's modulus.

As shown in Fig. 14, the difference between the analytical predictions from Eq 15 and the experimental data is ~3% for the transverse bends and 6% for the longitudinal bends. The lower the r_p/t ratio, the larger the disagreements of the K_S values. This seems reasonable. Because the r_p/t ratio is small, say <5, the transverse stress may become significant, and the pure bending theory, which ignores the transverse stress, may no longer be accurate enough to govern the bending behavior. The larger disagreement in the longitudinal bend data is somewhat confused. As indicated in the tensile data, a larger amount of work hardening is in the longitudinal direction than that of the transverse. According to the general observation, with the same Young's modulus, larger work hardening should generate larger springback or smaller K_S, as predicted. However, the measurement data indicate that larger work hardening creates larger K_S values, opposite to the predictions. Originally, it was thought that some mistakes may have occurred in specimen preparation; two additional batches of the CuNiBe sheets were, therefore, examined to make sure that the data obtained in the first batch are not an exceptional case. However, the majority of the data from all three batches shows that the springback factors for the longitudinal bends are indeed 2 to 5% higher than that of the transverse bends. The remaining two data at $r_p/t = 3.4$ show their transversal values higher than that of longitudinal bends. This inconsistency between prediction and measurements should be investigated further.

The predictions from Eq 25 are also compared with the experimental data shown in Fig. 15. Equation 15 is based on the assumptions that the effect of the nonlinear strain generated by large bending deformation can be neglected, whereas Eq 25 includes the nonlinear strain. As shown, the predictions from Eq 25 agree better with the measurements than those from Eq 15. As expected, the equation considering nonlinear strains provides better predictions; however, the difference is insignificant if the ratio of r_p/t is small. The predictions based on different formulations, Eq 15, 16, 21, and 25, are also reported in Fig. 16 and 17 for the longitudinal and transverse bend directions, respectively. As shown, the result differences between Eq 15 and 25 becomes <1% for r_p/t ratio <10, but rises to 5% for $r_p/t = 20$. Note that the series used to calculate the plastic moment, M_p, in Eq 25 converges very rapidly. In fact, only two to three terms are enough to have a convergent solution. Figure 18 shows the convergent behavior of the series solution for $r_p/t = 10$ and indicates that the difference between solutions with two and three terms is <0.02%.

In sheet bending, the plane strain condition is closer to reality, and should be the case adopted. Whereas Eq 15 is based on the plane strain assumption, Eq 16 is derived by assuming under plane stress deformation. The disagreement between Eq 15 and 16 may be regarded as the difference between wide sheet and narrow beam bending. As shown in Fig. 16 or 17, the differences for all calculations are ±2%, and the springback factors based on Eq 16 are lower. In other words, wide sheet bending has larger springback than narrow sheet bending. This is consistent with most of the observations (Ref 6, 13).

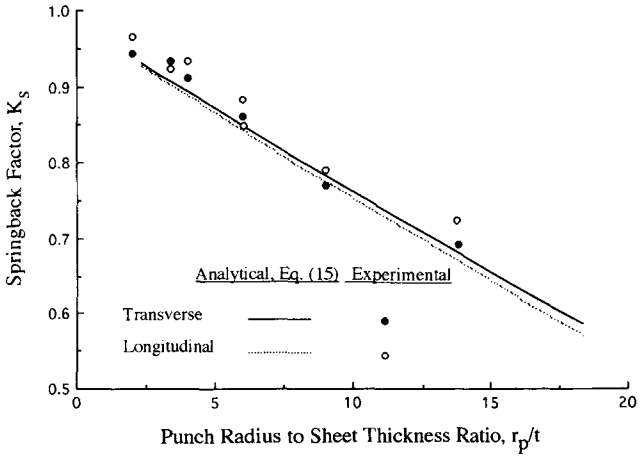

Fig. 14 Comparison between measurements and predictions by Eq 15

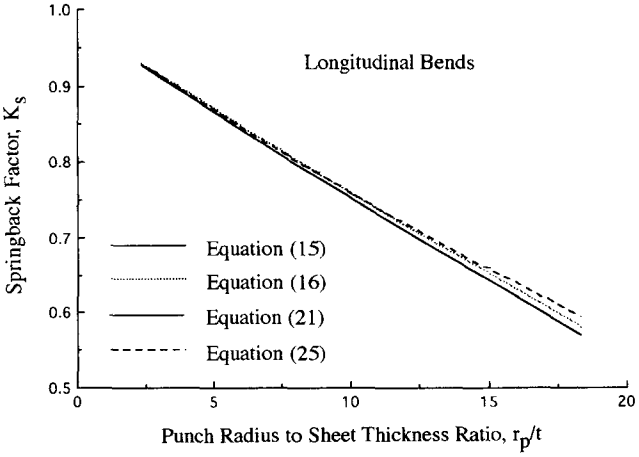

Fig. 16 Springback prediction with four different formulations for longitudinal bends

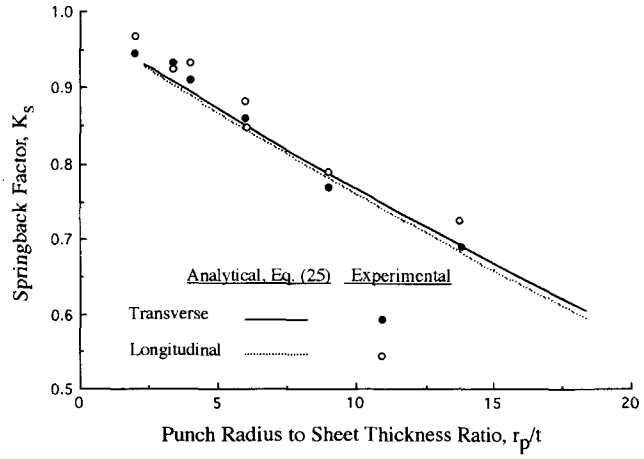

Fig. 15 Comparison between measurements and predictions by Eq 25

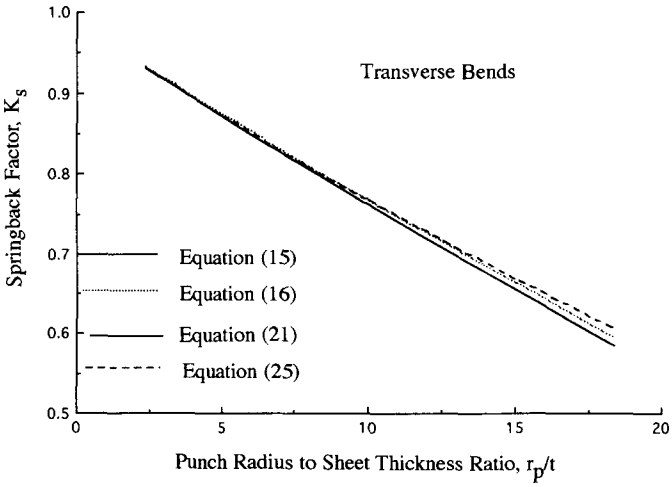

Fig. 17 Springback prediction with four different formulations for transverse bends

The difference between the results based on Eq 15 and those of Eq 21 are considered the elastic core effect. As shown, the differences between the cases by considering or not considering the elastic core are >0.2%. The equation considering the elastic core predicts a slightly higher springback factor, K_S. Because the bending moment is generated more effectively by the stresses away from the core region, the accuracy of the elastic stresses in the core region should only play a minor role in moment calculations. As expected, it has only a minor effect in the determination of springback. The above comparison study shows that although it is simple, Eq 15 is accurate enough to predict the springback behavior of CuNiBe sheets. The more complicated formula, Eq 17, is not necessarily providing better predictions than Eq 15.

The adoption between Eq 15 and 25 is somewhat dependent on the r_p/t ratio. As mentioned earlier, the result differences between Eq 15 and 25 become insignificant for r_p/t <10. Therefore, for r_p/t not too large, say <15, the simple formula of Eq 15 is appropriate.

6.2 *Bendability Results*

Currently, sheet bendability is rated by the minimum bend ratio. As the name implies, the bending test characterizes the ability of a material to be bent to a required geometry without failure. It is determined by a series of 90° bend tests. Following a bend test, the surface of the bent sheet is examined for cracks on the convex side of the radius. If no cracks are visible, the sample passes the test at that radius. The punch radius is then reduced, and another sheet sample is tested. This procedure is repeated until cracks appear on the sample surface. The smallest radius, R, not causing visible cracking is divided by the sheet thickness to determine the minimum bend ratio (R/t).

The CuNiBe sheets were tested to determine their minimum bend ratios in both the transverse and longitudinal bend directions. The results are shown in Table 4. The experimental data indicate that, while the longitudinal bend has better bendability compared to the transverse bend, the difference is insignificant. The photomicrographs for bent sheets at an r_p/t ratio near 3.0

Table 4 Bending properties of C17510 sheets

Alloy	Typical springback, K_S		Specimen(a)	Critical	
	Measurement	Prediction	r_p/t ratio	R/t ratio	Rating
C17510-TH04-T(b)	0.691 ± .030	0.689	13.76	2.0	Moderate
C17510-TH04-L(c)	0.724 ± .023	0.676	13.82	2.0	Moderate

(a) Specimen size: 75-mm long and 25-mm wide. Punch radius: r_p = 1.829 mm. (b) Transverse bend direction. (c) Longitudinal bend direction

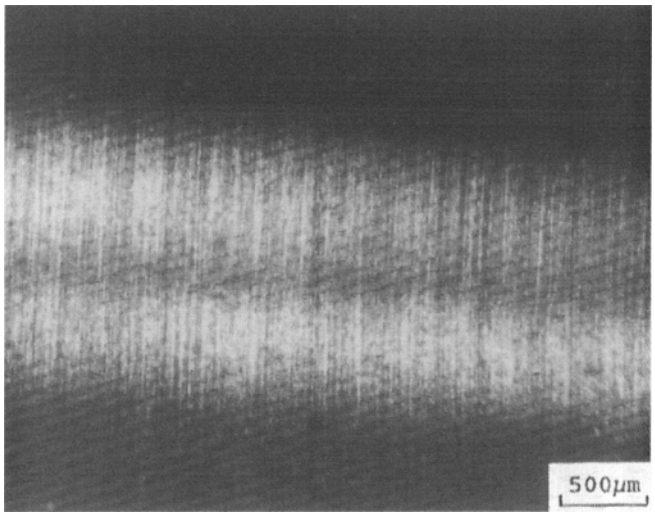

Fig. 18 Numerical convergence study

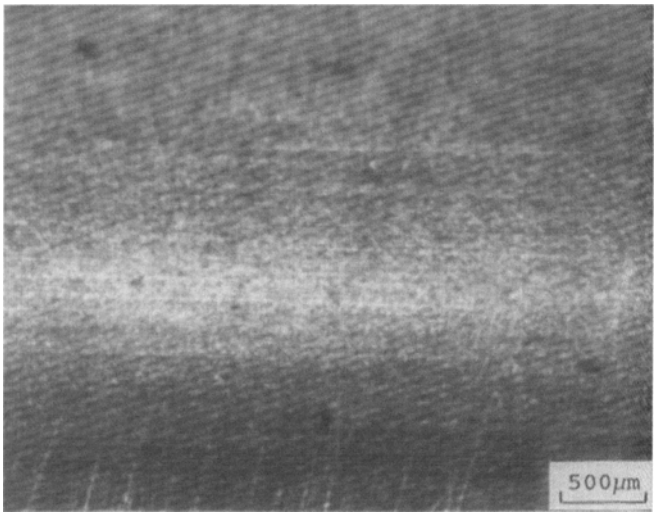

Fig. 19 Photomicrograph of a 90° longitudinal bend

are shown in Fig. 19 and 20, respectively. The bends were examined at 30× magnification, as required by most industrial specifications. Both bends show no fractures, although orange peel and superficial surface breaks do appear.

As in Table 4, the ratings of excellent, very good, and good are commonly used in industry. A sheet with an excellent rating can usually be used for deep draw and severely cupped or formed parts. The rating of very good is for moderately drawn or cupped parts. The good rating indicates that the sheet is formable to a 90° bend around a radius <3 times stock thickness. In fabrication, if the angle is acute, then a larger radius may be required. Sometimes multiple bending operations, instead of just one, will produce tighter bends than the minimum bend ratio indicates (Ref 5, 6, 12).

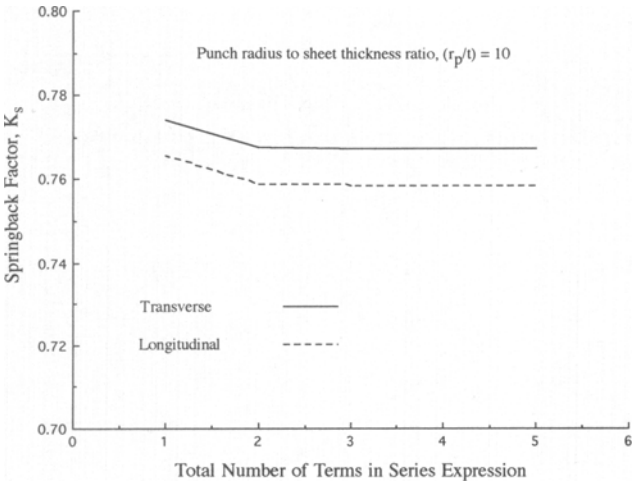

Fig. 20 Photomicrograph of a 90° transverse bend

6.3 *SEM Fractographical Analysis*

Longitudinal and transverse bending tests (sharp 180° bend) were conducted, and the fracture surfaces were investigated. The as-received rolled surface reveals many rolling marks along the rolling direction. Figure 21 shows that the rolled surface is considerably rough and that the rolling grooves can be as wide as 2 microns. Figure 22 shows the fracture surfaces of both the longitudinal and transverse bent specimens. Clearly, the cracks in the transverse bend specimen are deeper than in the longitudinal bend specimen. Because the rolling marks may cause the stress concentration and they are normal to the bending stress, they tend to develop deep cracks into the thickness of the sheet metal. See Fig. 23. The number of deep cracks for a transverse bend specimen is somewhat limited because the cracks localize themselves at high-stress concentration areas where the rolling marks are deeper. Figure 23 shows that shearing dimples are the major features deep down inside of the crack. However, irregular wavy fracture occurs near the rolled surface due to the complicated stress concentration condition caused by the rolling marks. See Fig. 24.

Figure 22(a) shows the surface of a longitudinal bend specimen containing numerous cracks. Interestingly, these cracks are shallower than those in the transverse bend specimens. This is due to the fact that, in the longitudinal bend specimen, the rolling marks are parallel to the maximum bending stress, and do not cause severe local stress concentrations. Therefore, the whole surface has the same opportunities to form shallow cracks, which are less detrimental. As the result, the longitudinal bend specimens produce better resistance to crack initiation and propagation. Occasionally, limited deep cracks occur in the longitudinal bend specimen. Its fracture surface is similar to that in the transverse bend specimen; i.e., shear dimple is the major feature inside of the deep crack. To summarize, both transverse and longitudinal bending specimens show cracks on the rolling surfaces after bending. The longitudinal bend specimen shows more small cracks than the transverse bend specimen. Nevertheless, the cracks in the transverse bend specimen are deeper than those in the longitudinal bend specimens.

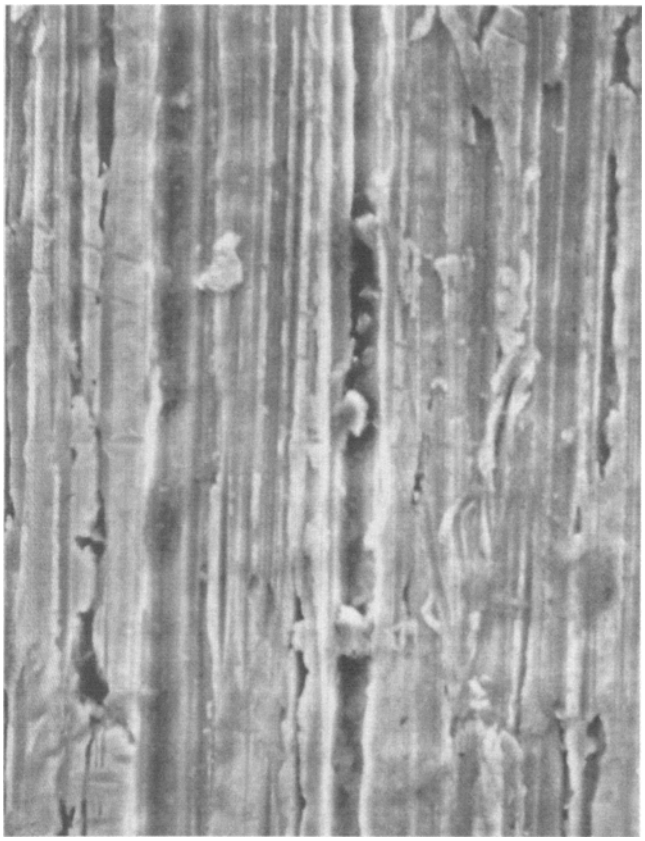

Fig. 21 SEM micrograph showing rolling marks on the surface of as-received specimen

6.4 *Optical Metallurgical Analysis of Bent Specimens*

The specimens of 180° bend tests were mounted, ground, polished, and etched for metallurgical analysis on the transverse plane. Both longitudinal and transverse bend specimens were investigated, and the results are discussed as follows.

Figure 25 contains three micrographs at different sections of a longitudinal bend specimen. It shows that grains are significantly deformed after bending. Due to the irregularity on the rolling surface and the limitation of the optical microscope, the cracks on the rolling surface are not readily revealed unless the cracks are reasonably long. Among three etched surfaces, as shown in Fig. 25, only Fig. 25(c) reveals two small cracks, one near the outer side surface and the other near the inner side surface. A higher magnification micrograph near the outer surface of Fig. 25(c), shows that the crack is aligned with the grain boundary, as shown in Fig. 26. It indicates that the crack has a tendency to initiate intergranually. Because the size and occurrence of cracks are limited, longitudinal bend specimens have good resistance to crack development.

Three micrographs of a transverse bend specimen are shown in Fig. 27 for comparison. Because all three micrographs show cracks, they indicate that the transverse bend specimen is more susceptible to developing deep cracks under bending stress. As discussed in the previous section, the rolling

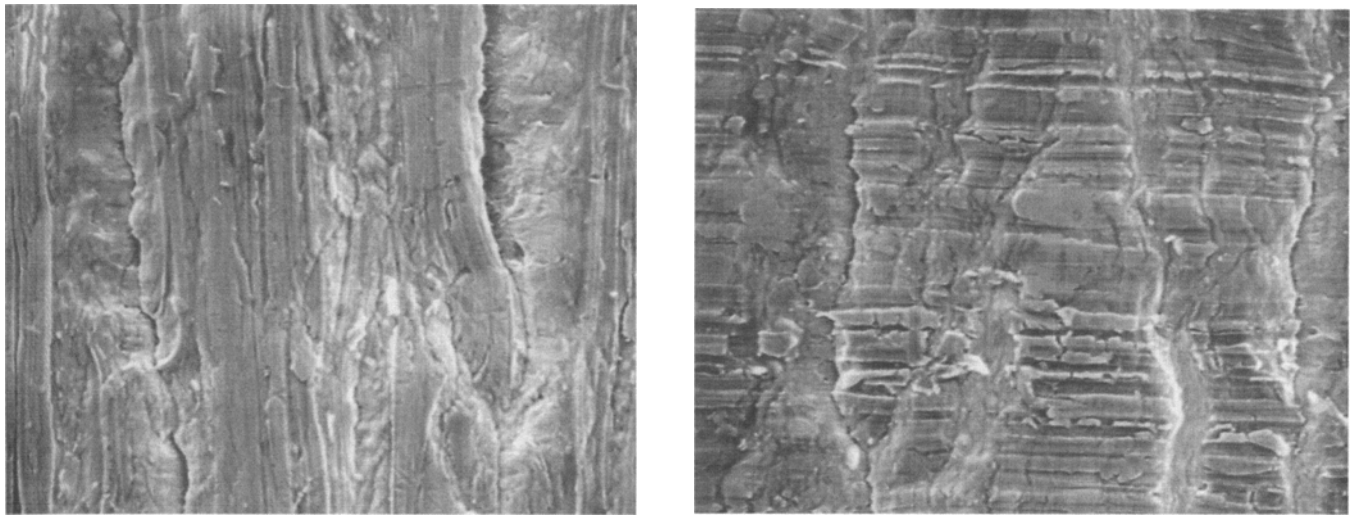

(a) (b)

Fig. 22 SEM fractographs of 180° bend specimens. (a) Longitudinal (b) Transverse

Fig. 23 SEM fractograph showing deep crack on a 180° transverse bend specimen

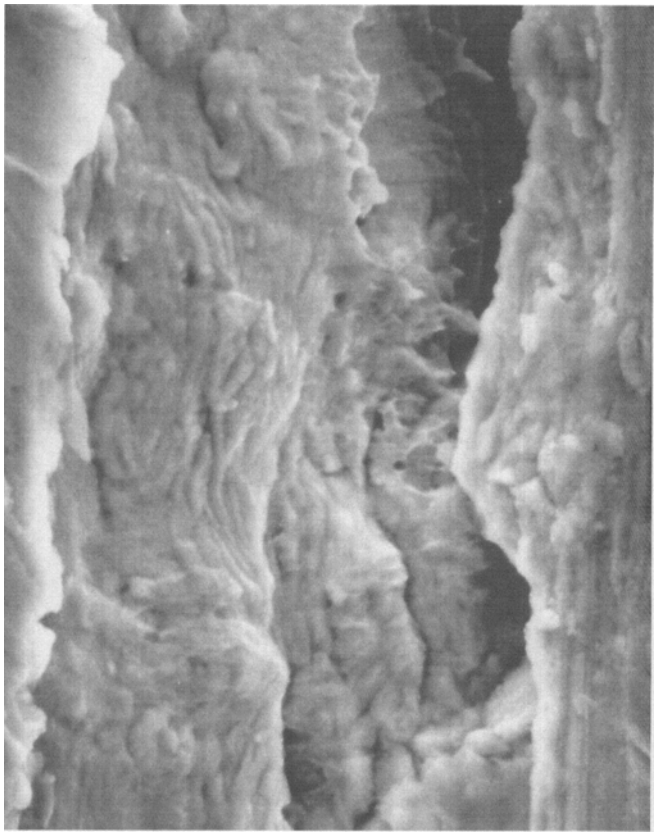

Fig. 24 SEM fractograph showing irregular features near rolling surface of a 180° transverse bend

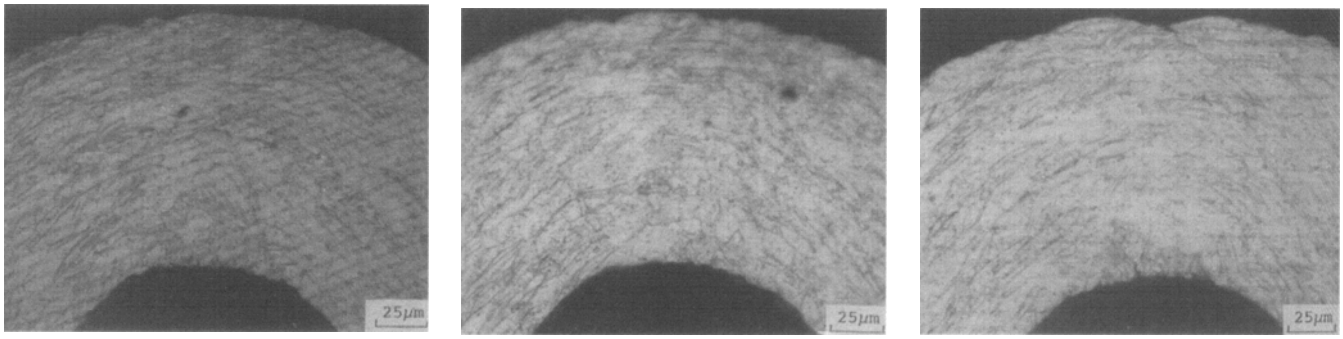

(a) (b) (c)

Fig. 25 Optical micrographs of cracks in 180° longitudinal bend specimen. (a) Section A (b) Section B (c) Section C

marks, which cause stress concentrations, will open deep cracks. Figure 27(a) shows a long crack grow transgranually from the outer surface. Figure 28 is a micrograph at higher magnification for the small crack on the outer surface of Fig. 27(c). It shows that the tip of this small crack is aligned with a grain boundary. This behavior is identical to that in the longitudinal bend specimen. Therefore, regardless of the types of bending specimens, cracks tend to initiate along the grain boundaries at an early stage when they are small and then grow transgranually through the thickness under higher bending stress.

Effort was made to investigate whether the beryllide stringers would initiate or affect the crack path for the bending specimens. No evidence was found that cracks prefer to grow along or through the beryllide stringers. This is probably due to the fact that the stringers are normal to the crack propagation direction, and the maximum bending stress is somewhat localized at a confined region near the bending area. Therefore, the crack is unlikely to align itself along the stringers direction. The beryl-

lide stringers would be more detrimental for a sheet metal under the tensile loading condition than under the bending condition. As mentioned in section 3, Tensile Testing, the stringers tend to weaken the transverse tensile strength.

7. Concluding Remarks

Bending is one of the major operations in sheet forming; it is often the major feature, especially in forming connectors for electrical and electronic applications. This paper studies the forming and fractographical characteristics of a CuNiBe sheet. The forming-related tensile properties were first examined. Apparatus for a bending test was developed to evaluate the springback behavior, as well as its bendability. An interchangeable punch block was designed and built to accommodate the multiple radii needed for the bend test.

As indicated in the tensile testing data, the constitutive relationship for the CuNiBe sheets closely follows a power-law curve. Four different analytical solutions based on the power-law constitutive relationship were developed to predict the springback at bending conditions. The analytical predictions were first compared with the measurement as well as with each other to identify an appropriate formula to be used in design of the highly reliable spring components. The simple form of Eq 15 was found to be adequate to the ratio of $r_p/t \leq 10$. However, if the ratio $r_p/t > 15$, the series solution, Eq 25 should be used. Because only two to three terms are needed to have a converged solution, no heavy computation effort is needed to obtain the series solution. With the quantitative springback information obtained from the analytical solutions, presented appropriate tooling can be designed to compensate for the springback, such as overbending the sheet. Some other antispringback bending operations, including bottoming, stretch bending, and multistep bending, can also be used.

Reasonably good agreements were found between the testing data and analytical predictions on springback behavior. In general, based on the analytical formulations, the higher the yield strength, the lower the springback factor or the higher the springback for sheets with the same Young's modulus. However, the CuNiBe sheets behave somewhat differently. The sheet in the longitudinal direction having higher yield strength and work hardening, creates a higher springback factor than that of the transverse direction. This inconsistency between the prediction and measurement is still not fully understood and should be investigated further.

Note that three batches of sheets were tested. Although these three batches are of the same grade, some differences exist from batch to batch. The inconsistency among the measurements or between the predictions and measurements may be partially due to the differences of the material characteristics associated with the three batches of sheets supplied. In fact, this is one of the major problems in industry; i.e., the consistency of springback obtained with the same grade of sheets, but from different batches or suppliers. This consistency evidently depends on the scatter of the alloy characteristics and the tooling. In order to determine the significance of such variations, the present formulas are perhaps the most effective tools to use because with the formulations, the influence of the major material and tooling parameters can be determined. The former includes the Young's modulus, yield strength, strain-hardening parameters, and Poisson ratio. The latter involves the punch radius, punch speed, sheet thickness, and sheet width.

The sheet bendability characterized by the minimum bend ratio was also studied. The bendability information is intended to be used as a guide when selecting the appropriate material for an application. The 90° bends were also examined at 30×

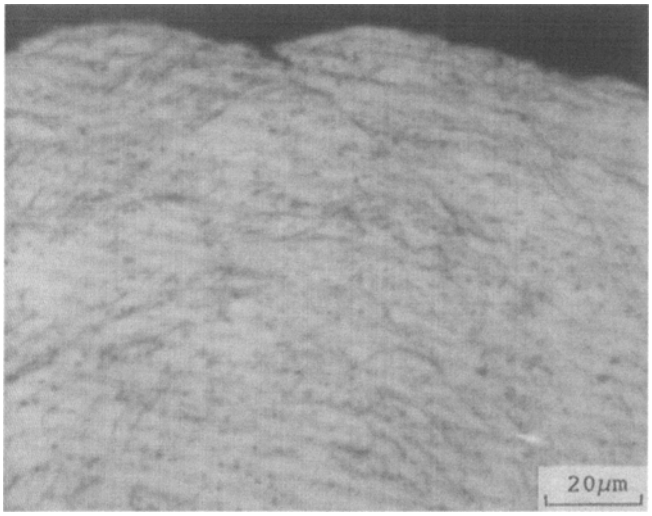

Fig. 26 Higher magnification of Fig. 25(c). Showing an intergranular crack near the outer surface

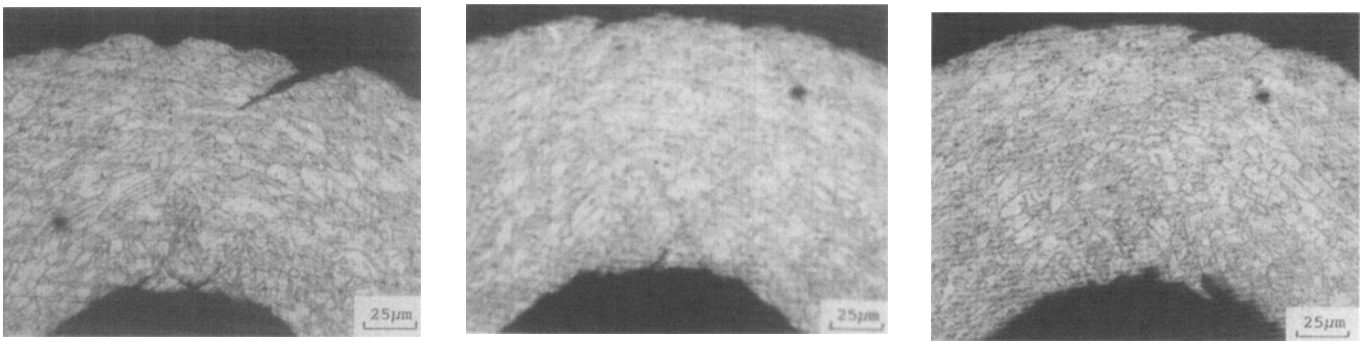

(a) (b) (c)

Fig. 27 Optical micrographs showing cracks in a 180° transverse bend specimen. (a) Section A (b) Section B (c) Section C

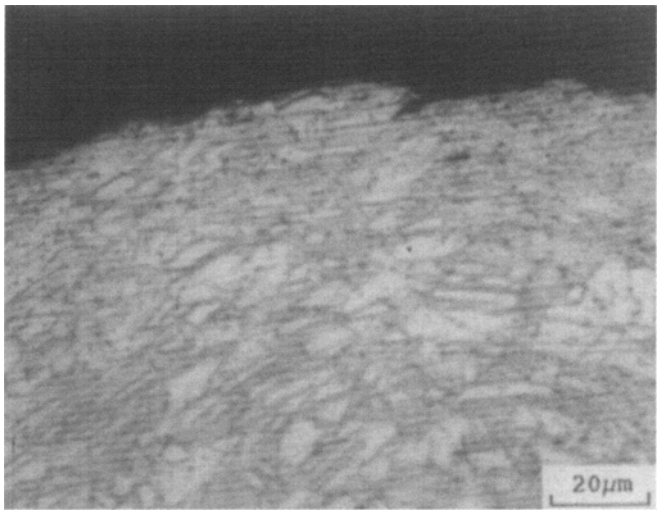

Fig. 28 Higher magnification of Fig. 27(c). Showing intergranular crack near the outer surface

magnification as required by most industrial specifications. Both 90° bends at the minimum bend ratio show no fractures, although orange peel and superficial surface breaks do appear. In general, the longitudinal bend exhibits better bendability than the transverse bend.

The microstructure and fracture surfaces of this material were investigated using the optical metallurgical and SEM microscopes. The microstructure of this material contains beryllide phase, which is rich in Ni and Co. Many large beryllide stringers are in the shape of tadpoles as the result of the milling process. For the tensile specimen, the stringers are detrimental because cracks initiate at the stringer sites where very little plastic deformation is available. The stringers lower the tensile strength in the transverse direction because they are normal to the loading direction.

The rolled surface contains many rolling marks, which can cause stress concentrations. For the 180° bend specimens, evidence showed that these rolling marks create deeper cracks in the transverse bend specimen than in the longitudinal bend specimen. Therefore, the manufacturer should improve the surface quality on the milling surface. Under bending stress, a crack grows intergranually at its early stage and transgranularly when it is getting longer. Under bending stress, the beryllide stringers do not affect the crack path because they are aligned normal to the crack.

Acknowledgments

This work was partially sponsored by a grant provided by NGK Metals Corp., Reading, PA. The authors gratefully acknowledge the support. The authors wish to thank Y.V. Murty, AMP Inc., Harrisburg, PA, and F. Zhao and M. Brawley, Drexel University for their assistance in conducting this research.

References

1. ASTM B 534-91, Copper-Cobalt-Beryllium Alloy and Copper-Nickel-Beryllium Alloy Plate, Sheet, Strip, and Rolled Bar, *Annual Book of ASTM Standards*, Vol 02.01, American Society for Testing and Materials, 1992, p 644-646
2. A.A. Tseng, K.P. Jen, N.A. Gildersleeve, and T. Ochiai, A Formability Analysis of Beryllium Copper Strip, *IICIT Conn-Cept '92:25th Annual Connector and Interconnection Technology Symposium*, Int. Institute of Connector and Interconnection Technology, 1992, p 465-480
3. D. Williamson, Micromanufacturing at the Crossroad, *Manuf. Eng.*, Vol 95 (No. 6), 1985, p 34-40
4. A.A. Tseng, Materials Characterization and Finite Element Simulation for Forming Miniature Metal Parts, *Finite Elements in Analysis and Design*, Vol 6, 1990, p 251-265
5. C. Wick, J.T. Benedict, and R.F. Veilleux, Forming, *Tool and Manufacturing Engineers Handbook*, Vol 2, Ed., Society of Manufacturing Engineers, 1985, p 10.10-10.30
6. S. Kalpakjian, *Manufacturing Processes for Engineering Materials*, 2nd ed., Addison-Wesley, 1991
7. Metallography and Microstructure, *Metals Handbook*, 9th ed., Vol 9, American Society for Metals, 1985, p 393-395
8. G. Vander Voort, *Metallography: Principles and Practice*, McGraw-Hill, 1984, p 625
9. ASTM E 8M-86a, Methods of Tension Testing of Metallic Materials [Metric], *Annual Book of ASTM Standards*, Vol 03.01, American Society for Testing and Materials, 1987, p 199-222
10. ASTM E 646-78, Test Method for Tensile Strain-Hardening Exponents (n-Values) of Metallic Sheet Materials, *Annual Book of ASTM Standards*, Vol 03.01, American Society for Testing and Materials, 1987, p 704-711
11. A.K. Ghosh, S.S. Hecker, and S.P. Keeler, Sheet Metal Forming and Test, *Workability Testing Techniques*, G.E. Dieter, Ed., American Society for Metals, 1984, p 135-195
12. W.F. Hosford and R.M. Caddell, *Metal Forming: Mechanics and Metallurgy*, Prentice-Hall, 1983
13. C.A. Queener and R.J. De Angelis, Elastic Springback and Residual Stresses in Sheet Metal Formed by Bending, *Trans. ASM*, Vol 61, 1968, p 757-768